Supplementary Information for

Black Carbon Emissions Generally Underestimated in the Global South as Revealed by Globally Distributed Measurements

Yuxuan Ren[1*], Christopher R. Oxford[1], Dandan Zhang[1], Xuan Liu[1,2], Haihui Zhu[1], Ann M. Dillner[3], Warren H. White[4], Rajan K. Chakrabarty[1], Sina Hasheminassab[5], David Diner[5], Emmie Le Roy[1], Joshin Kumar[1], Valerie Viteri[1], Keyao Song[1], Clement Akoshile[6], Omar Amador-Muñoz[7], Araya Asfaw[8], Rachel Ying-Wen Chang[9], Diana Francis[10], Paterne Gahungu[11], Rebecca M. Garland[12,13], Michel Grutter[7], Jhoon Kim[14], Kristy Langerman[15], Pei-Chen Lee[16], Puji Lestari[17], Olga L. Mayol-Bracero[18], Mogesh Naidoo[12], Narendra Nelli[10], Norman O'Neil[19], Sang Seo Park[20], Abdus Salam[21], Bighnaraj Sarangi[18], Yoav Schechner[22], Robyn Schofield[23], Sachchida N. Tripathi[24,25], Eli Windwer[26], Ming-Tsang Wu[27,28], Qiang Zhang[29], Yinon Rudich[26], Michael Brauer[30], and Randall V. Martin[1]

[1]Department of Energy, Environmental & Chemical Engineering, Washington University in St. Louis, St. Louis, Missouri 63130, United States

[2]Scripps Institution of Oceanography, University of California San Diego, San Diego, California 92093, United States

[3]Air Quality Research Center, University of California Davis, Davis, California 95616, United States

[4]Crocker Nuclear Laboratory, University of California Davis, Davis, California 95616, United States

[5]Jet Propulsion Laboratory, California Institute of Technology, Pasadena, California 91109, United States

[6]Department of Physics, University of Ilorin, Ilorin, 240003, Nigeria

[7]Instituto de Ciencias de la Atmósfera y Cambio Climático, Universidad Nacional Autónoma de México, Mexico City, 04510, Mexico

[8]Institute of Geophysics and Space Science, Addis Ababa University, Addis Ababa, 1176, Ethiopia

[9]Department of Physics and Atmospheric Science, Dalhousie University, Halifax, Nova Scotia B3H 4R2, Canada
[10]Environmental and Geophysical Sciences Lab, Earth Science Department, Khalifa University, Abu Dhabi, 127788, United Arab Emirates
[11]Institute of Applied Statistics, University of Burundi, Bujumbura, BP1550, Burundi
[12]Council for Scientific and Industrial Research, Pretoria, 0001, South Africa
[13]Department of Geography, Geo-Informatics and Meteorology, University of Pretoria, Pretoria, 0002, South Africa
[14]Department of Atmospheric Sciences, Yonsei University, Seoul, 03722, Republic of Korea
[15]Department of Geography, Environmental Management and Energy Studies, University of Johannesburg, Johannesburg, 2006, South Africa
[16]Department of Public Health, National Cheng Kung University, Tainan, 701, Taiwan
[17]Faculty of Civil and Environmental Engineering, Bandung Institute of Technology, Bandung, 40132, Indonesia
[18]Department of Environmental Science, University of Puerto Rico, Puerto Rico, 00931, United States
[19]Department of Applied Geomatics, University of Sherbrooke, Sherbrooke, Quebec J1K 2R1, Canada
[20]Department of Urban and Environmental Engineering, Ulsan National Institute of Science and Technology, Ulsan, 44919, Republic of Korea
[21]Department of Chemistry, University of Dhaka, Dhaka, 1000, Bangladesh
[22]Department of Electrical Engineering, Technion Israel Institute of Technology, Haifa, 3200003, Israel
[23]School of Geography, Earth and Atmospheric Sciences, University of Melbourne, Melbourne, 3010, Australia
[24]Department of Civil Engineering, Indian Institute of Technology Kanpur, Kanpur, 208016, India

[25]Department of Sustainable Energy Engineering, Indian Institute of Technology Kanpur, Kanpur, 208016, India
[26]Department of Earth and Planetary Sciences, Weizmann Institute of Science, Rehovot, 76100, Israel
[27]Department of Family Medicine, Kaohsiung Medical University Hospital, Kaohsiung Medical University, Kaohsiung, 807, Taiwan
[28]PhD Program in Environmental and Occupational Medicine, Kaohsiung Medical University, Kaohsiung, 807, Taiwan
[29]School of Environment, Tsinghua University, Beijing, 100084, China
[30]School of Population and Public Health, University of British Columbia, Vancouver, British Columbia V6T 1Z3, Canada
[*]Email: ren.yuxuan@wustl.edu

Contents of this file

This Supplementary Information contains Text S1 and S2, Tables S1 to S3, and Figures S1 to S7.

Text S1. Statistics Calculation

We mainly use the coefficient of determination (r^2), normalized mean bias (NMB, Eq. 1), and normalized mean difference (NMD, Eq. 2) to evaluate simulated BC concentrations (C_{sim}) using coincident measurements (C_{meas}) across a total of N SPARTAN sites.

$$NMB = \frac{\sum_{i=1}^{N}(C_{sim,i} - C_{meas,i})}{\sum_{i=1}^{N} C_{meas,i}} \quad (1)$$

$$NMD = \frac{\sum_{i=1}^{N}|C_{sim,i} - C_{meas,i}|}{\sum_{i=1}^{N} C_{meas,i}} \quad (2)$$

where $C_{sim,i}$ is the simulated BC concentration at SPARTAN site i, $C_{meas,i}$ is the measured BC concentration at the same site, and $|C_{sim,i} - C_{meas,i}|$ is the absolute difference between the simulated and measured concentrations.

Text S2. Representativeness Bias

Differences in representativeness between measurements and simulations arise from comparing a point measurement with an area average, magnified by the tendency for measurements to be in locations with elevated BC concentrations[1-3]. To examine this potential bias, we perform GCHP sensitivity simulations at the finest available meteorological resolution of C720 (~12 km) and compare BC concentrations with those from simulations at C360 (~25 km) resolution in 2022, the year in which archival began of the GEOS-FP C720 meteorological data. A full-year simulation at C720 would be computationally prohibitive. However, a high level of consistency is found between BC concentrations in the C360 and C720 simulations (Figure S7), indicating that comparing BC simulations at approximately 25 km resolution with point measurements would yield similar results as using a 12 km simulation. The most prominent exception is for Beijing in January, where and when the C720 has BC concentrations that are 22% lower than at C360, partially explaining the anomaly apparent in Figure 2. Moreover, SPARTAN stations are mostly located on rooftops with a mean height of 17 m, which

97 increases their spatial fetch (Table S1), generally reducing differences between volume-
98 averaged modeled concentrations and point measurements.

Tables

Table S1. Location information of SPARTAN sites used in this study.

Site	Host Institute	Latitude	Longitude	Rooftop Height (m)
Abu Dhabi	Masdar Institute	24.44	54.62	27
Addis Ababa	Addis Ababa University	9.01	38.82	3
Bandung	Institute of Technology Bandung	-6.89	107.61	30
Beijing	Tsinghua University	40.00	116.33	9
Bujumbura	University of Burundi	-3.38	29.38	12
Dhaka	Dhaka University	23.73	90.40	22
Fajardo	Cabezas de San Juan Nature Reserve	18.38	-65.62	4
Haifa	Technion Israel Institute of Technology	32.78	35.02	32
Halifax	Dalhousie University	44.64	-63.59	13
Ilorin	Ilorin University	8.48	4.67	11
Johannesburg	University of Johannesburg	-26.18	28.00	11
Kanpur	Indian Institute of Technology Kanpur	26.51	80.23	8
Kaohsiung	Kaohsiung Medical University	22.65	120.31	15
Melbourne	University of Melbourne	-37.80	144.96	57
Mexico City	Universidad Nacional Autónoma de México	19.33	-99.18	16
Pasadena	Jet Propulsion Laboratory	34.20	-118.17	15
Pretoria	Council for Scientific and Industrial Research	-25.76	28.28	13
Rehovot	Weizmann Institute	31.91	34.81	16
Seoul	Yonsei University	37.56	126.93	25
Sherbrooke	Sherbrooke University	45.38	-71.93	9
Taipei	National Taiwan University	25.04	121.50	10
Ulsan	Ulsan National Institute of Science and Technology	35.58	129.19	12

Table S2. Sampling information and BC concentration (μg/m^3) for SPARTAN sites used in this study.

Site	Start Date	Most Recent Sample Date	Sampling Seasons[a]	Start Date for MAIA Sites[b]	*N*[c]	Mean (Median)	Standard Error
Abu Dhabi	4/26/2019	12/23/2023	DJF, MAM, JJA, SON		113	2.7 (2.7)	0.11
Addis Ababa	12/7/2022	12/27/2023	DJF, MAM, JJA, SON	12/7/2022	116	4.8 (4.5)	0.19
Bandung	9/6/2019	7/11/2021	DJF, MAM, JJA, SON		23	3.7 (3.9)	0.20
Beijing	3/24/2020	11/28/2023	DJF, MAM, JJA, SON	8/30/2022	153	1.4 (1.3)	0.090
Bujumbura	12/9/2022	12/26/2023	DJF, MAM, JJA, SON		18	3.7 (3.2)	0.40
Dhaka	8/11/2020	10/7/2023	MAM, JJA, SON		52	5.6 (5.4)	0.86
Fajardo	3/18/2021	12/24/2023	DJF, MAM, JJA, SON		34	0.11 (0.083)	0.017
Haifa	2/16/2022	6/17/2023	DJF, MAM, JJA, SON	2/16/2022	143	0.85 (0.63)	0.10
Halifax	6/14/2019	10/24/2023	DJF, MAM, JJA, SON		112	0.23 (0.21)	0.015
Ilorin	7/13/2019	12/1/2021	DJF, MAM, JJA, SON		36	3.0 (2.2)	0.61
Johannesburg	4/7/2022	12/28/2023	DJF, MAM, JJA, SON	4/7/2022	168	2.4 (2.3)	0.18
Kanpur	7/14/2021	5/24/2022	DJF, MAM, JJA		14	3.8 (3.0)	0.73
Kaohsiung	8/20/2022	12/29/2023	DJF, MAM, JJA, SON	8/20/2022	123	1.3 (1.4)	0.12
Melbourne	8/9/2022	12/28/2023	DJF, MAM, JJA, SON		34	0.43 (0.32)	0.061
Mexico City	2/26/2021	12/24/2023	DJF, MAM, JJA, SON		52	2.1 (2.0)	0.11
Pasadena	11/9/2021	11/15/2023	DJF, MAM, JJA, SON	11/9/2021	233	0.47 (0.44)	0.030
Pretoria	10/22/2020	12/27/2023	DJF, MAM, JJA, SON	4/15/2021	233	2.1 (2.0)	0.24
Rehovot	7/2/2020	6/7/2023	DJF, MAM, JJA, SON	11/5/2021	178	1.2 (1.0)	0.11
Seoul	9/11/2020	12/30/2023	DJF, MAM, JJA, SON		65	1.2 (1.1)	0.094
Sherbrooke	8/29/2019	6/21/2023	DJF, MAM, JJA, SON		67	0.36 (0.28)	0.049
Taipei	1/27/2022	12/31/2023	DJF, MAM, JJA, SON	1/27/2022	218	0.83 (0.75)	0.040
Ulsan	10/28/2021	12/23/2023	DJF, MAM, JJA, SON		92	0.78 (0.74)	0.043

[a] DJF includes December, January, and February; MAM includes March, April, and May; JJA includes June, July, and August; SON includes September, October, and November.

[b] These sites began using the MAIA sampling protocol on the specified date.

[c] *N* is the number of samples from each site included in this study.

Table S3. Sampling information and BC concentration for other individual measurements referenced in this study. Mass absorption cross section (MAC, m^2/g) values at 880 nm and estimated values at 633 nm are provided for measurements using aethalometers when available.

Country	Site	Latitude	Longitude	Location Type	Instrument	MAC at 880 nm (m^2/g)	MAC at 633 nm (m^2/g)[a]	Sampling Period	BC ($\mu g/m^3$)	Source
Argentina	Buenos Aires	-34.56	-58.51	suburban	Aethalometer (AE42)	16.6	23.1	Nov 2014 to Mar 2016	3.18	Resquin et al.[4]
Bolivia	La Paz	-16.50	-68.13	urban	Aethalometer (AE33)	7.77	10.8	Jan to Jun, 2018	1.6	Mardoñez-Balderrama et al.[5]
Ivory Coast	Lamto	6.22	-5.03	rural	Aethalometer (AE31)	16.6	23.1	Jan 2015 to May 2017	1.4	Kouassi et al.[6]
Mexico	Monterrey	25.75	-100.26	urban	Aethalometer (AE33)	16.6	23.1	Jan to Dec, 2016	2.46	Peralta et al.[7]
Morocco	Kenitra city	34.23	-6.61	urban	Aethalometer (AE31)	16.6	23.1	July 2020 to Feb 2021	0.9	Bounakhla et al.[8]
Peru	Hyo	-12.04	-75.32	rural	Aethaometer (AE33)	7.77	10.8	May 2022 to Oct 2023	0.65	Villalobos-Puma et al.[9]
Rwanda	Kigali	-1.96	30.06	urban	Portable Black Carbon Monitors (BC1060)	NaN	NaN	Jan to Dec, 2020	7.8	Kalisa and Adams[10]
Mozambique	Manhiça	-25.41	32.81	semi-rural	Sunset OC-EC Aerosol Analyzer	NaN	NaN	2014 to 2015	0.9	Curto et al.[11]
Cotonou	Benin	6.35	-2.43	urban	Thermal/Optical Carbon Analyzer (DRI Model 2001)	NaN	NaN	Feb 2015 to Mar 2017	2	Djossou et al.[12]
Ivory Coast	Abidjan	5.33	-4.02	urban	Thermal/Optical Carbon Analyzer (DRI Model 2001)	NaN	NaN	Feb 2015 to Mar 2017	7	Djossou et al.[12]

[a] In aethalometer studies, MAC measurements at 880 nm are typically used to calculate BC concentrations[4]. For direct comparison, we adjust the MAC values to 633 nm, the wavelength used in Hybrid Integrating Plate/Sphere (HIPS) measurements in SPARTAN. This adjustment assumes that MAC varies inversely with wavelength and that the particles are small relative to the wavelength[13].

Figures

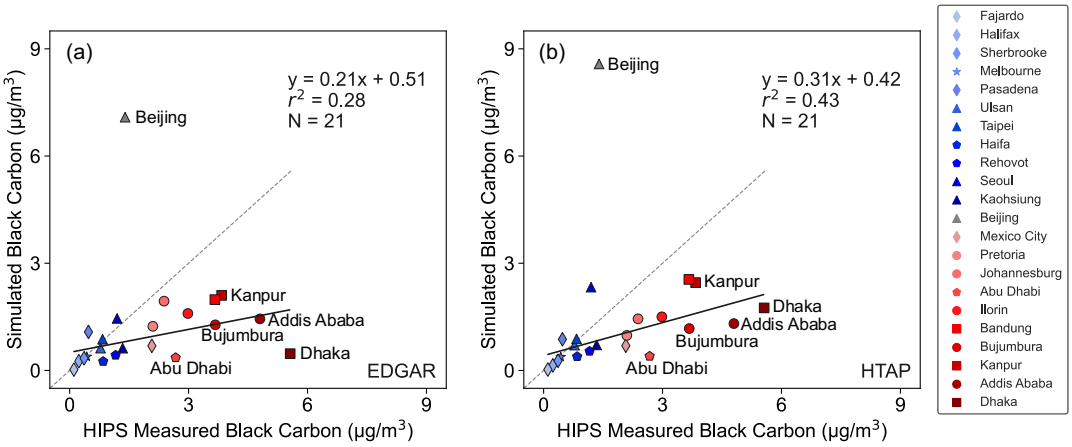

Figure S1. Annual mean BC concentrations across SPARTAN sites, with GCHP simulations using different inventories at C360 resolution (~25 km) in 2019 and SPARTAN measurements from 2019 to 2023. (a) EDGAR and (b) HTAP. Annotations include the line of best fit (y), coefficient of variation (r^2), and number of comparison points (N). The lowest half of the measured concentrations are indicated in blue and the upper half in red. The Beijing site, marked in grey, is excluded from statistical calculations due to anomalies in its emissions estimates. Symbols indicate different regions (diamonds for North America, star for Australia, triangles for East Asia, pentagons for the Middle East, circles for Africa, and squares for South Asia).

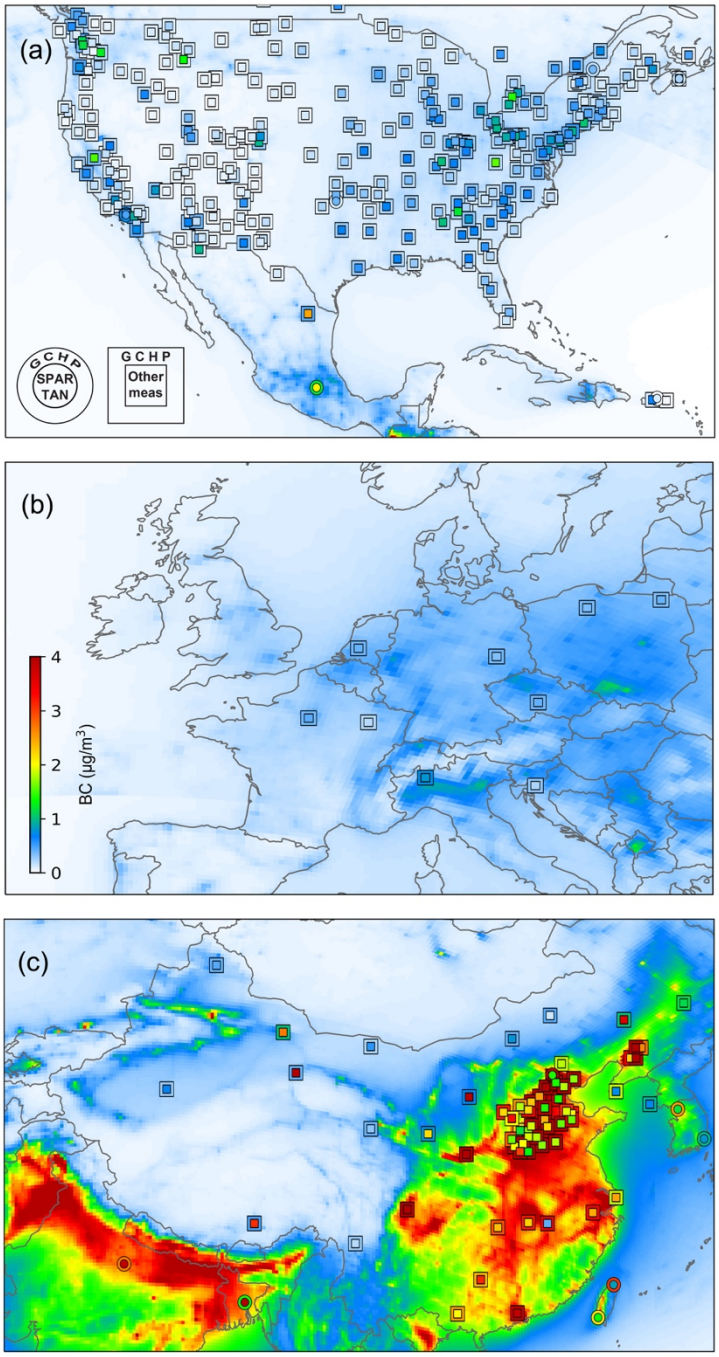

Figure S2. BC concentrations from measurements and simulations across different regions: (a) North America, (b) Europe, and (c) East Asia. SPARTAN and additional measurements are represented by colored circles and squares, respectively, surrounded by concentric circles and squares indicating local GCHP concentrations using the CEDS inventory. A GCHP C360 (~25 km) simulation using the CEDS inventory is in the background.

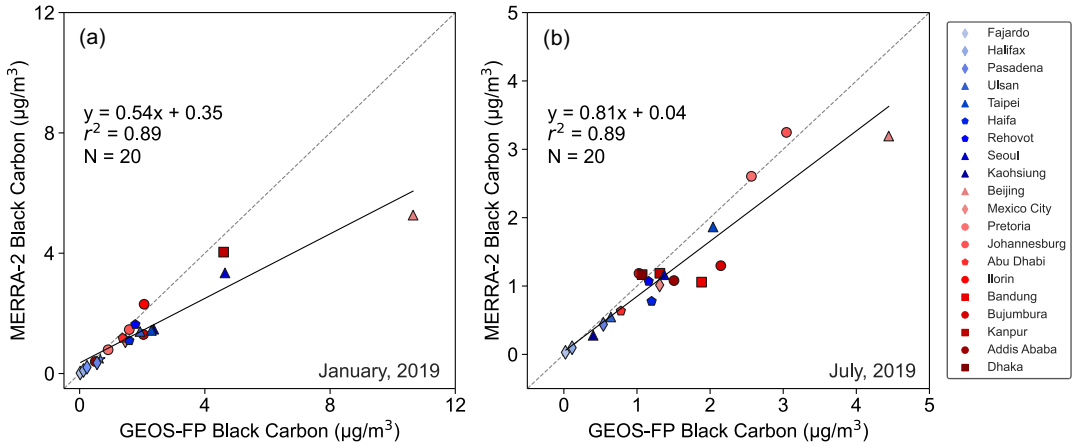

Figure S3. Mean BC concentrations across SPARTAN sites, with GCHP simulations using different meteorology (GEOS-FP vs MERRA-2) at C180 resolution (~50 km) in 2019. (a) January and (b) July. Annotations include the line of best fit (y), coefficient of variation (r^2), and number of comparison points (N). Symbols indicate different regions (diamonds for North America, triangles for East Asia, pentagons for the Middle East, circles for Africa, and squares for South Asia).

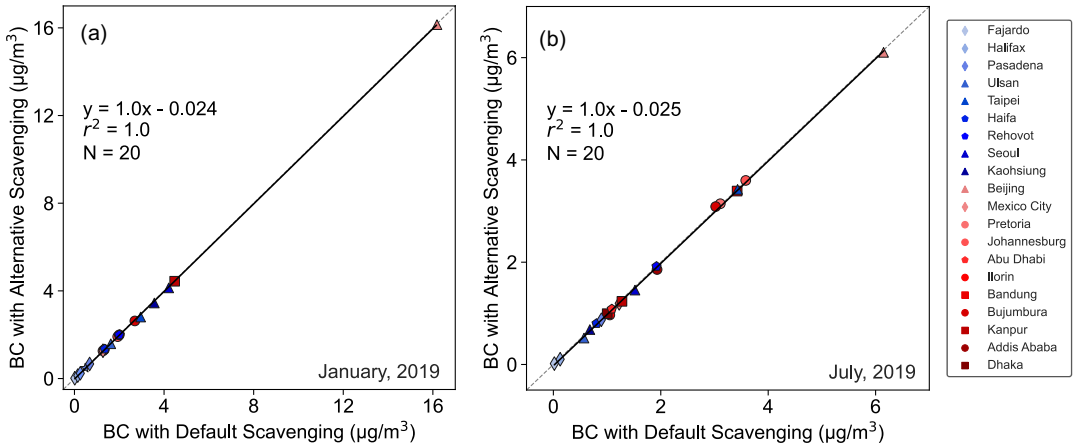

Figure S4. Mean simulated BC concentrations across SPARTAN sites, with GCHP simulations using alternative scavenging at C360 resolution (~25 km) in 2019. (a) January and (b) July. Annotations include the line of best fit (y), coefficient of variation (r^2), and number of comparison points (N). Symbols indicate different regions (diamonds for North America, triangles for East Asia, pentagons for the Middle East, circles for Africa, and squares for South Asia).

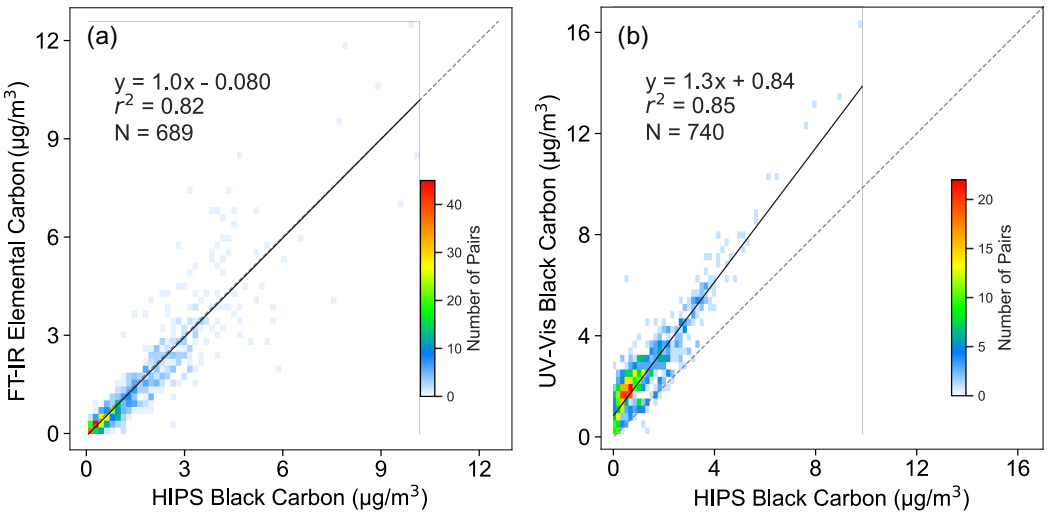

Figure S5. Comparison of BC concentrations measured by HIPS, FT-IR, and UV-Vis in SPARTAN. (a) HIPS vs FT-IR and (b) HIPS vs UV-Vis. Annotations include the line of best fit (y), coefficient of variation (r^2), and number of comparison points (N).

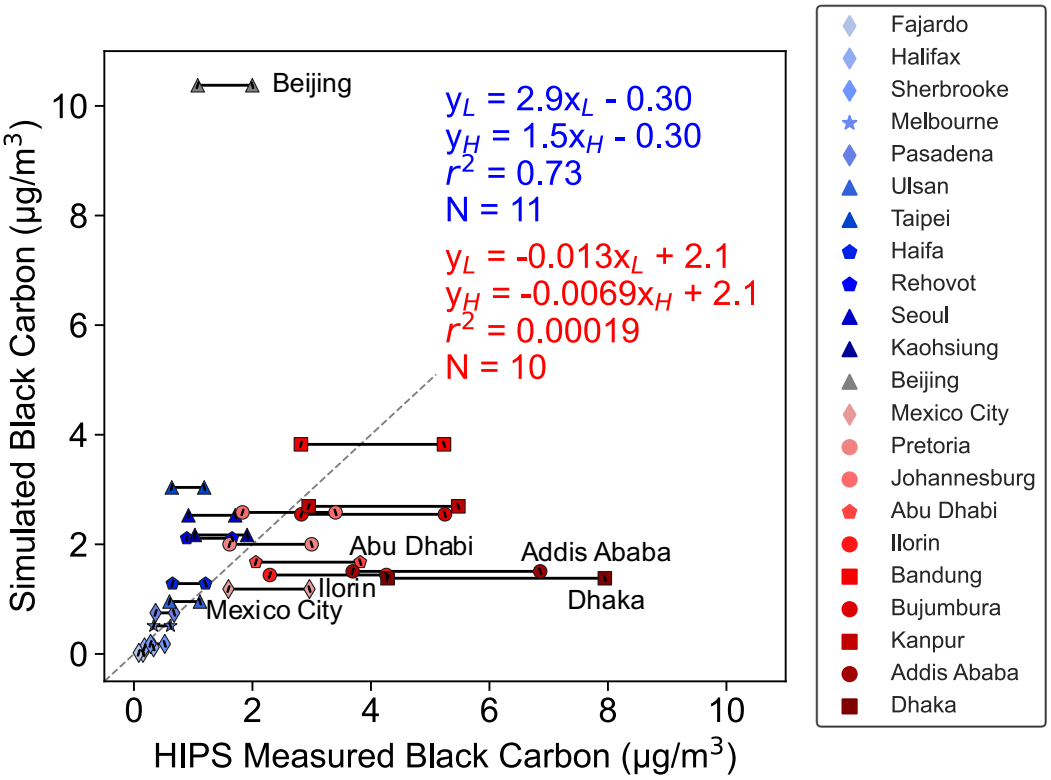

Figure S6. Annual mean BC concentrations across SPARTAN sites, with GCHP simulations using the CEDS inventory and HIPS measurements using varying MAC values from 7 m^2/g to 13 m^2/g. The simulations are from 2019, while the measurements are from 2019 to 2023. Annotations include the line of best fit (y), coefficient of variation (r^2), and number of comparison points (N). A MAC of 7 m^2/g is represented by leftmost markers filled with a forward slash and a line of best fit (y_L) indicating lower BC concentrations, while a MAC of 13 m^2/g is represented by rightmost markers filled with a backslash and a line of best fit (y_H) indicating higher BC concentrations. The lowest half of the measured concentrations are indicated in blue and the upper half in red. The Beijing site, marked in grey, is excluded from statistical calculations due to anomalies in its emissions estimates. Symbols indicate different regions (diamonds for North America, star for Australia, triangles for East Asia, pentagons for the Middle East, circles for Africa, and squares for South Asia).

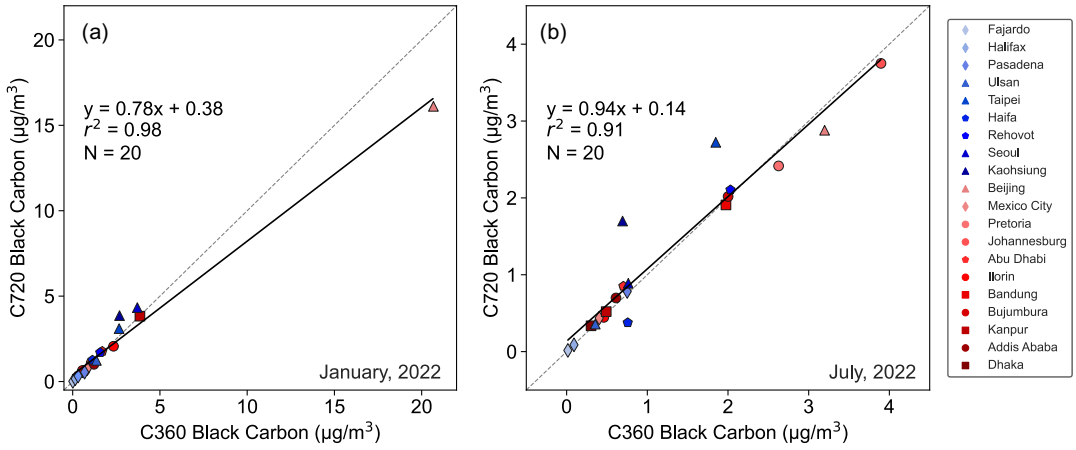

Figure S7. Mean simulated BC concentrations across SPARTAN sites, with GCHP simulations using the CEDS inventory at C360 (~25 km) and C720 (~12 km) in 2022. (a) January and (b) July. Annotations include the line of best fit (y), coefficient of variation (r^2), and number of comparison points (N). Symbols indicate different regions (diamonds for North America, triangles for East Asia, pentagons for the Middle East, circles for Africa, and squares for South Asia).

References

1. Gilardoni, S., Vignati, E. & Wilson, J. Using measurements for evaluation of black carbon modeling. *Atmos. Chem. Phys.* **11**, 439–455 (2011).
2. Swall, J. L. & Foley, K. M. The impact of spatial correlation and incommensurability on model evaluation. *Atmos. Environ.* **43,** 1204–1217 (2009).
3. Wang, R. et al. Spatial representativeness error in the ground-level observation networks for black carbon radiation absorption. *Geophys. Res. Lett.* **45,** 2106–2114 (2018).
4. Resquin, M. D. et al. Local and remote black carbon sources in the Metropolitan Area of Buenos Aires. *Atmos. Environ.* **182,** 105–114 (2018).
5. Mardoñez-Balderrama, V. et al. Atmospheric black carbon in the metropolitan area of La Paz and El Alto, Bolivia: concentration levels and emission sources. *Atmos. Chem. Phys.* **24,** 12055–12077 (2024).
6. Kouassi, A. et al. Measurement of atmospheric black carbon concentration in rural and urban environments: cases of Lamto and Abidjan. *J. Environ. Prot.* **12,** 855–872, (2021).
7. Peralta, O. et al. Atmospheric black carbon concentrations in Mexico. *Atmos. Res.* **230,** 104626 (2019).
8. Bounakhla, Y. et al. Black carbon aerosols at an urban site in North Africa (Kenitra, Morocco). *Atmos. Pollut. Res.* **13,** 101489 (2022).
9. Villalobos-Puma, E. et al. Atmospheric black carbon observations and its valley-mountain dynamics: eastern cordillera of the central Andes of Peru. *Environ. Pollut.* **355,** 124089 (2024).
10. Kalisa, E. & Adams, M. Population-scale COVID-19 curfew effects on urban black carbon concentrations and sources in Kigali, Rwanda. *Urban Clim.* **46,** 101312 (2022).
11. Curto, A. et al. Predictors of personal exposure to black carbon among women in southern semi-rural Mozambique. *Environ. Int.* **131,** 104962 (2019).
12. Djossou, J. et al. Mass concentration, optical depth and carbon composition of particulate matter in the major southern West African cities of Cotonou (Benin) and Abidjan (Cote d'Ivoire). *Atmos. Chem. Phys.* **18,** 6275–6291 (2018).